# *Ab initio* study of metal-organic framework-5 $Zn_4O(1,4\text{-benzenedicarboxylate})_3$: An assessment of mechanical and spectroscopic properties

M. Mattesini,* J. M. Soler, and F. Ynduráin
*Departamento de Física de la Materia Condensada, Universidad Autónoma de Madrid, E-28049, Spain*
(Received 2 November 2005; revised manuscript received 14 December 2005; published 13 March 2006)

The electronic structure of porous metal-organic framework-5 (MOF-5) of composition $Zn_4O(1,4\text{-benzenedicarboxylate})_3$ was investigated with an *ab initio* density-functional-theory method. The unit cell volume and atomic positions were optimized with the well-known local-density approximation leading to a good agreement between the experimental and theoretical equilibrium structural parameters. Single crystal elastic constants ($C_{11}$, $C_{12}$, and $C_{44}$) were then computed at the athermal limit in order to estimate fundamental figures for technological and engineering applications. Our calculations suggest that MOF-5 behaves as a soft and ductile material with a Young's modulus of the order of Oak wood. Particular attention was also focused on the study of oxygen, and carbon *K* XANES spectra. The differences in their shapes and energy peak positions were discussed in relation to the bonding topology and to the different calculational methods used.

DOI: 10.1103/PhysRevB.73.094111 PACS number(s): 62.20.Dc, 71.15.Mb, 61.10.Ht

## I. INTRODUCTION

Metal-organic frameworks (MOFs)[1] are currently considered among the most promising materials for applications[2] in gas storage (e.g., $H_2$ and $CH_4$), catalysis, and molecular recognition. Of special interest is the fact that MOFs represent an innovative and appealing alternative for storing molecular hydrogen.[3] Looking towards a future socioeconomic scenario based on nonfossil fuels a new material that can adsorb large amounts of $H_2$ gas, at ambient temperature and at relatively low pressures, is of great relevance for the development of hydrogen-fueled vehicles. In this context, it is worth noting that hydrogen exhibits the highest heating value per mass of all chemical fuels and that it is regenerative. A clean way to produce hydrogen from water is, for instance, to use the sunlight in combination with photovoltaic cells and electrolysis.[4] However, the real advancement in $H_2$ storage systems not only depends on the sorption capacity of the supporting material but also on its mechanical properties. Hydrogen gas must be adsorbed on safe systems that are satisfying certain technical requirements, such as hardness and elasticity, which are important factors in determining the durability of the storing material. It is in this mechanical framework that we developed our investigation.

Among various MOFs structures the metal-organic framework-5 represents one of the most interesting systems. This structure (Fig. 1) consists of octahedral Zn-O-C clusters joined together by benzene linkers to build a cubic three-dimensional framework that has an *exceptionally rigid*[1] and highly porous structure.[2,5,6] Recently, it has also been shown that both size and chemical functionality of the MOFs pores can be systematically engineered to augment the surface area and therefore the $H_2$ uptake.[5] This is the case of similar metal-organic framework-6 and -8 (IRMOF-6 and -8) that have been shown to uptake double and quadruple the amount of hydrogen.[5] Nonetheless, our efforts were here focused on the smaller MOF-5 system since it represents a reference model phase that can be studied with *ab initio* methods at reasonable computational costs. The main purpose of this paper is therefore to model the electronic, structural, and mechanical characteristics of the metal-organic framework-5 of composition $Zn_4O(1,4\text{-benzenedicarboxylate})_3$ by using attested first-principles techniques. First, elastic properties were described by means of the calculation of the complete set of inequivalent elastic constants. Important technological numbers such as stiffness and ductility were then estimated by computing the polycrystalline bulk modulus that accounts for the spatially averaged electron density, and the shear modulus that, on the other hand, is more sensitive to the nonuniform distribution of the electron density. Furthermore, we report a complete spectroscopic characterization of the x-ray absorption fingerprints of MOF-5 that can be used as a precious reference in the synthesis of this material.

The outline of the paper is as follows. In Sec. II we give a brief review of the computational scheme used. The calcu-

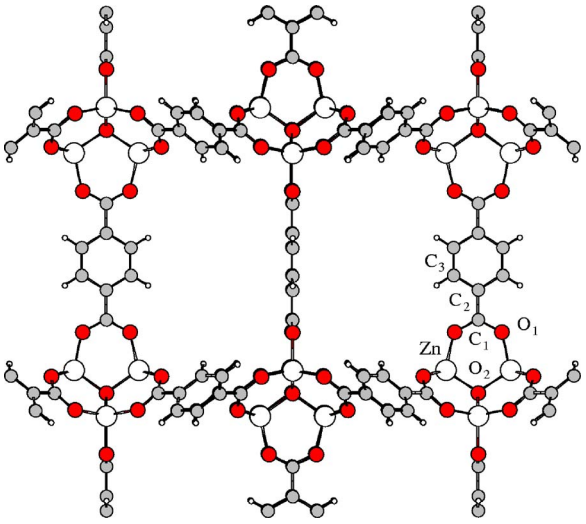


FIG. 1. (Color online) Unit cell of cubic MOF-5 structure along the direction of the [110] plane. Zinc, oxygen, and carbon are depicted in white (large white spheres), red (dark gray), and gray (light gray), respectively. Hydrogen atoms are drawn with small white spheres.

 

lations of the structural and electronic properties are developed in Sec. III. The computation of the single crystal elastic constants is described in Sec. IV, while the calculated x-ray absorption spectra are discussed in Sec. V. Finally, conclusions are drawn in Sec. VI.

## II. DETAILS OF CALCULATIONS

Our calculations were performed within the local density approximation (LDA) of density-functional theory[7] (DFT), using the SIESTA package.[8,9] We used the parametrization of Perdew and Zunger[10] for the exchange-correlation functional and norm-conserving Troullier-Martins pseudopotentials[11] in the Kleinman-Bylander factorized form.[12] The employed reference configurations were $4s^2 4p^0 3d^{10} 4f^0$, $2s^2 2p^4 3d^0 4f^0$, $2s^2 2p^2 3d^0 4f^0$, and $1s^1 2p^0 3d^0 4f^0$ for Zn, O, C, and H, respectively. The cutoff radius for the $s$, $p$, $d$, and $f$ components of the pseudopotentials were $2.15a_o$ for Zn, $1.15a_o$ for O, and $1.25a_o$ for both C and H. To describe the valence electrons we used an atomic orbitals basis set consisting of finite-range numerical pseudoatomic wave functions in the line of Sankey and Niklewski.[13] The finite range of the orbitals was defined by an orbital confinement energy[9] of 50 meV. In the present calculations we used a double-$\zeta$ basis set with polarization orbitals on all the atoms. The resulting $k$-grid for Brillouin zone (BZ) sampling was chosen according to the Monkhorst-Pack[14] scheme, which yielded eight $k$-points in full BZ.

## III. STRUCTURAL AND ELECTRONIC PROPERTIES

The equilibrium structural parameters of MOF-5 were obtained by a conjugate gradient minimization of the total energy with respect to the atomic positions and lattice constants. Atomic forces were calculated using a variation of the Hellman-Feyman theorem including Pulay corrections[9] to account for the local character of the basis set. In our study, the residual atomic forces were less than 0.05 eV Å$^{-1}$ and the stress tolerance less than 0.5 GPa. Close agreement was achieved between the calculated zero-pressure lattice constant and the x-ray diffraction data of the fully desolvated MOF-5 single-crystal at 169±2 K (Table I). The relaxed atomic positions were also consistent with the measured single-crystal properties.

The total electronic density of states (DOS) was computed for MOF-5 at its equilibrium geometry. The obtained DOS is shown in Fig. 2. The calculated LDA band gap ($E_g$) amounts to 2.5 eV, which indicates that MOF-5 is at the borderline between the definition of insulating and semiconducting materials. However, being the LDA band structures well-known to underestimate the gap in semiconductors, it is then reasonable to expect an experimental $E_g$ value larger than 2.5 eV. Such a theoretical shortcoming amounts generally to 30–50% of the experimental band gaps and can be attributed to the ground-state formalism of the DFT.[15] The overall electronic properties of MOF-5 are basically marked by the presence of the $Zn_4O$ clusters that bring to the MOF-5 structure the character of a wide band gap semiconductor (ZnO), and by the proximity of the benzenedicarboxylate linkers, which on the other hand tend to enhance a semimetallic behavior. The electronic delocalization effect introduced by the 1,4-benzenedicarboxylate (BDC) groups breaks off with the presence of insulating $Zn_4O$ corners, thus leading to an opening of the band gap in the porous structure. The connection between inorganic corners and organic linkers is further disclosed by the computed partial density of states (PDOS). From the PDOS shown in Fig. 3 we see that at the top of the valence band (VB) the Zn 3$d$-states hybridize with the 2$p$-states of O and C, while the bottom of the conduction band (CB) is primarily determined by the unoccupied $s$- and $p$-orbitals of O, C, and Zn. The top of the VB has the typical conformation of the bulk ZnO system,[16] where the Zn $d$-states hybridize strongly with the $p$-orbitals of the oxygen atoms. Both $O_1$ and $O_2$ 2$p$ wave functions are energetically close to the Zn 3$d$-states, which implies a significantly strong interaction between these atoms. Furthermore, it is in this energy region where the electronic states of the $Zn_4O$ corners mix up together with those of the BDC fragments to form a stable MOF-5 crystal. The electronic linkage between these two moieties is exemplified by the hybridization of the $s,p$-states of $O_1$ and $C_1$ in the energy regions −12/0 eV and −22/−18 eV. The middle VB region consists of narrow bands with small gaps that are originated from the flat molecular crystal-like band structure of MOF-5. These occupied $s$-states belong to the carbon atoms of the BDC linkers and their indented DOS shape reminds one very much of that of $C_{60}$.[17] Finally, the bottom of the VB shows localized oxygen and carbon wave functions with $s$- and $p$-character.

The unoccupied part of the PDOS is mainly composed by $s,p$-orbitals of O, C, and Zn, which are characterizing the x-ray absorption properties of the MOF-5 crystal. In particular, by considering the dipole approximation the absorption $K$-shells of carbon and oxygen are determined by the shape and energy position of the empty $p$-states. The CB of atom type $O_1$ consists of two sharp $\pi^*$ peaks in the lower portion of the empty bands and of a more broaden higher energy

TABLE I. Optimized lattice parameters and atomic positions (in fractional coordinates) for the MOF-5 structure.

| Property | LDA | Expt.[a] |
|---|---|---|
| Crystal system | Cubic | Cubic |
| Space group | $Fm\bar{3}m$ (225) | $Fm\bar{3}m$ (225) |
| Atoms/cell (fcc) | 106 | 106 |
| $a_o$ (Å) | 25.888 | 25.885 |
| $V_o$ (Å$^3$) | $17.35\times10^3$ | $17.34\times10^3$ |
| $\rho$ (g/cm$^3$) | 0.589 | 0.590 |
| Atom type | Atomic positions $(x,y,z)$ | |
| $Zn_1$ (32$f$) | (0.207,0.207,0.207) | (0.206,0.206,0.206) |
| $O_1$ (96$k$) | (0.219,0.219,0.133) | (0.219,0.219,0.134) |
| $O_2$ (8$c$) | (0.250,0.250,0.250) | (0.250,0.250,0.250) |
| $C_1$ (8$g$) | (0.111,0.251,0.251) | (0.112,0.250.0.250) |
| $C_2$ (48$g$) | (0.053,0.251,0.251) | (0.054,0.250,0.250) |
| $C_3$ (96$k$) | (0.217,0.217,0.025) | (0.218,0.218,0.026) |
| $H_1$ (96$k$) | (0.191,0.191,0.048) | (0.194,0.194,0.045) |

[a]Experimental data from Ref. 2.

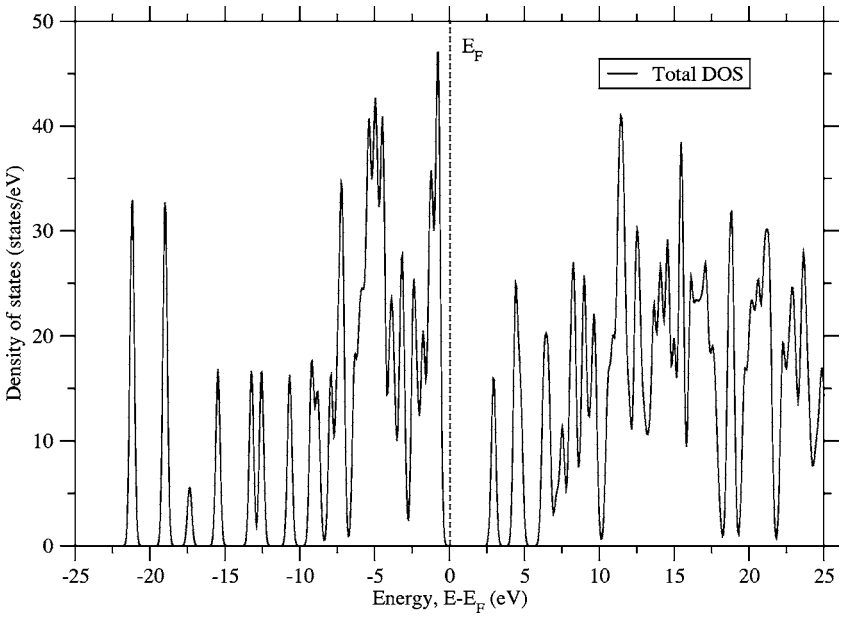


FIG. 2. Calculated total density of states for MOF-5.

region of *s*- and *p*-states with a $\sigma^*$ character. On the other hand, atom $O_2$ has only a few $\sigma^*$ peaks in its CB as to indicate the absence of the double bonding. Such an electronic feature comes from the fact that atom $O_1$ is involved in a $sp^2$-like bonding with atom $C_1$, whereas $O_2$ shows a pure $sp^3$ hybridization with the surrounding Zn ions. This electrostructural diversity leads to important differences in the *K*-shell fingerprints of the two oxygen types as will be shown later in Sec. V. In the same manner we can now describe the CB's shape of atoms $C_1$, $C_2$, and $C_3$. All the unoccupied PDOSs of carbon atoms have the bottom of the CB determined by the *p*-states with $\pi^*$ character, while the higher energy portion presents the participation of both *s*- and *p*-orbitals with $\sigma^*$ nature.

## IV. CALCULATIONS OF THE SINGLE-CRYSTAL ELASTIC CONSTANTS

In what follows, we illustrate the calculation of the elastic constants ($C_{ij}$), which determine the stiffness of a crystal against an externally applied strain. They can be computed by applying small strains to the equilibrium unit cell and determining the corresponding variations in the total energy. The necessary number of strains is imposed by the crystal symmetry[18] of the investigated material. In the case of the cubic MOF-5 structure the elastic moduli can be divided into two different classes, the bulk modulus $B=(C_{11}+2C_{12})/3$, and the two shear moduli, $C_{11}-C_{12}$ and $C_{44}$. The bulk modulus is related to the curvature of the energy-volume data set $[B=VE''(V_i)]$, and can be computed by making the least-

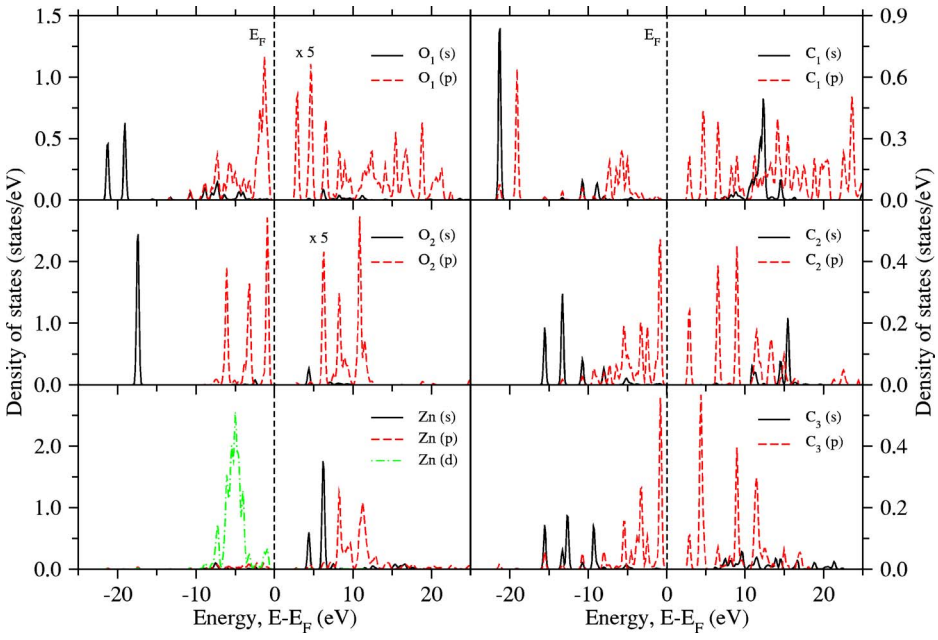


FIG. 3. (Color online) Calculated partial density of states for MOF-5. Note that the CBs of $O_1$ and $O_2$ were multiplied by a factor of 5 for a better comparison with Fig. 5.

TABLE II. Calculated zero-pressure elastic constants (GPa) of MOF-5. Relaxation of the internal degrees of freedom was carried out for all the applied deformations.

| $B$ ($B'$) | $C_{11}$ | $C_{12}$ | $C_{44}$ | $G_H$ | $B/G_H$ |
|---|---|---|---|---|---|
| 17.02 (3.61) | 21.52 | 14.77 | 7.54 | 5.46 | 3.12 |

squares fit of the calculated $E(V_i)$ data with the Birch type equation of state.[19] The other two elastic moduli can be deduced by straining the lattice vectors with the volume-conserving tetragonal and orthorhombic shears.[20] From the $C_{ij}$ values reported in Table II one can see that the entire set of calculated elastic constants satisfies the conditions imposed by the Born stability criteria[21] for a cubic crystal,[20] pointing therefore to a mechanically stable MOF-5 phase. The elastic properties of such a metal-organic system can be understood by looking first at its structural topology. This structure is made of highly porous organic frameworks held together by strong metal-oxygen-carbon bonds. The linkage between the metal oxide group ($Zn_4O$) and the organic moiety (BDC) generates a rather soft material with relatively small elastic moduli. The calculated bulk modulus clearly indicates that the MOF-5 is an easily compressible system with an isotropic $B$ value one order of magnitude smaller than that of a pure ZnO structure.[22,23] Its compressibility is mostly determined by the presence of the BDC linkers which offer almost the same kind of resistance to an external strain as found for graphite.[24]

The main difference between single crystal systems described in *ab initio* calculations and isotropic polycrystalline samples resides in the disorder of the grain orientations. A practical way to provide first-principles parameters of such polycrystalline systems is to compute single crystal values first and then to transform them into macroscopic quantities by using appropriate averaging procedures. For instance, an averaged bulk and shear modulus can be determined by combining values of the single-crystal $C_{ij}$ according to the proper symmetry relations. For cubic lattices, the averaged bulk modulus is equivalent to the single-crystal value, while the shear modulus is bounded from above by the Voigt approximation[25] and from below by the Reuss approximation.[26] Here we adopt Hill's averaging method,[27] where the shear modulus ($G_H$) is obtained through an arithmetic means of the two extremes [$G_H=(G_V+G_R)/2$]. The polycrystalline bulk and shear moduli represent two fundamental figures for technological and engineering applications that can be used to predict the brittle and ductile behavior of materials. In 1954 Pugh[28] introduced the ratio of the bulk modulus to shear modulus by considering $B$ as the resistance to fracture and $G$ the resistance to plastic deformation. With such an assumption a high (low) $B/G_H$ value was therefore associated to ductility (brittleness) and the critical number which separates brittle and ductile was fixed at about 1.75. From the calculated $B/G_H$ ratio of Table II it is evident that MOF-5 behaves as a ductile material. However, one should expect that after $H_2$ loading the MOFs structures will manifest the so-called hydrogen embrittlement phenomenon that has already been observed in other hydrogen storage systems.[29,30]

Three more numbers are important for technological applications: the Young's modulus $E$, the elastic anisotropy $A$, and the Poisson's ratio $\nu$. The first one is defined as the ratio between linear stress and strain and is used to provide a measure of the stiffness of the solid, i.e., the larger the value of $E$, the stiffer is the material. The Young's modulus can be calculated by using Hill's shear and bulk moduli through the following equation:

$$E = \frac{9BG_H}{3B + G_H}. \tag{1}$$

The computed Young's modulus amounts to 14.8 GPa, which is a rather small value, typical of soft materials such as Oak wood. The elastic anisotropy of crystals has an important implication in engineering science since it is highly correlated with the probability to induce microcracks.[31] The anisotropy factor for cubic crystals,[32] $A=(2C_{44}+C_{12})/C_{11}$, has therefore been evaluated to provide insight on the elastic anisotropy of the MOF-5 compound. For a completely isotropic material the $A$ factor takes the value of one, while values smaller or greater than unity measure the degree of elastic anisotropy. The computed value is 1.39, thus pointing to the presence of a certain anisotropicity. This finding indicates that the durability of the MOF-5 system as a gas storage material can be considerably reduced by the formation of microcracks.

The investigation of the elastic properties can be completed by providing the Poisson's ratio, which quantifies the stability of the crystal against shear. This ratio can formally take values between $-1$ and 0.5, which corresponds, respectively, to the lower limit where the material does not change its shape (e.g., special types of polymer foams or cork), and to the upper limit where the volume remains unchanged (e.g., liquid or rubber). Poisson's ratio can be defined using the Hill's limits by the following equation:

$$\nu = \frac{3B - 2G_H}{2(3B + G_H)}. \tag{2}$$

The $\nu$ value obtained from our theoretical studies (0.36) is very close to $\frac{1}{3}$, which is the usual magnitude for isotropic[33] homogeneous substances. The Poisson ratio also provides information about the type of bonding forces. For systems with predominantly central interatomic interactions (i.e., ionic and Van der Waals crystals) the Poisson's ratio is usually close to 0.25.[34,35] Therefore the calculated value of 0.36 for MOF-5 suggests that in such a compound the interatomic forces are noncentral. This is also confirmed by the violation of the Cauchy relation for a cubic system ($C_{12} \neq C_{44}$). The covalent character of the MOF-5 is given by the presence of the BDC groups that bring a certain amount of torsional and bending (i.e., angular) forces into the system.

Finally, for polycrystalline aggregates one can also estimate the values of the average longitudinal ($v_l$) and shear ($v_s$) sound velocities from the Hill's equations as follows:

$$v_l = \sqrt{\left(B_H + \frac{4}{3}G_H\right)\rho} \tag{3}$$

and

TABLE III. The LDA density ($\rho$ in g/cm$^3$), longitudinal, transverse, average sound velocity ($v_l$, $v_s$, and $v_m$ in km/s), and the Debye temperature ($\theta_D$ in K) obtained from the average sound velocity.

| $\rho$ | $v_l$ | $v_s$ | $v_m$ | $\theta_D$ |
|---|---|---|---|---|
| 0.589 | 6.42 | 3.03 | 3.41 | 294.62 |

$$v_s = \sqrt{\frac{G_H}{\rho}}. \tag{4}$$

Furthermore, the mean sound velocity can be computed by combining Eqs. (3) and (4) and can be defined as

$$v_m = \left[\frac{1}{3}\left(\frac{2}{v_s^3} + \frac{1}{v_l^3}\right)\right]^{-1/3}. \tag{5}$$

The Debye temperature $\theta_D$, which is proportional to the average sound velocity, can be obtained by the equation[36]

$$\theta_D = \frac{h}{k}\left[\frac{3n}{4\pi}\left(\frac{N_A\rho}{M}\right)\right]^{1/3} v_m, \tag{6}$$

where $h$ is the Plank's constant, $k$ the Boltzmann's constant, $N_A$ the Avogadro's number, $\rho$ the density, $M$ the molecular weight, and $n$ the number of atoms in the unit cell. The Debye temperature gives information about the lattice vibrations and is a relevant parameter in characterizing material properties such as the "rigidity" of the lattice.[37] Our first-principles calculations suggest that MOF-5 has a relative low $\theta_D$ value as to indicate that it is a rather flexible system. The calculated sound velocities and Debye temperature values are shown in Table III.

## V. X-RAY ABSORPTION NEAR EDGE STRUCTURE (XANES)

X-ray absorption spectroscopy (XAS) is a powerful tool for investigating the electronic structure of materials by probing the angular momentum content of the unoccupied electronic states. Herein, we report on the theoretical study of O and C *K* absorption edges of cubic MOF-5 structure. The employed calculational scheme (FDMNES package[38,39]) uses either the multiple-scattering theory (MST)[40] or the finite difference method (FDM) to solve the Schrödinger equation. Both methods were used here to describe the propagation of the excited photoelectron through the investigated system. The first approach is based on the solution of the Dyson equation with a complex self-energy of the Hedin-Lundqvist[41] type for the single-particle Green's function. The MST has been widely used to calculate the electronic structure of a wide variety of materials by using the so-called muffin-tin approximation (MTA). On the other hand, the FDM formalism applied to XANES spectroscopy consists of the creation of a three-dimensional grid in a spherical volume centered on the absorbing atom, and solving the Schrödinger equations by discretizing them over the node points of the selected grid. With this technique it is then possible to work with a free shape potential and thus avoid the MTA. Going beyond a spherical averaged potential with a constant interstitial value is an important requirement for an accurate investigation of loosely packed structures such as that of the cubic MOF-5. However, one of the main drawbacks of the FDM method is that it is highly CPU consuming so that we can use it only for small cluster sizes. Therefore calculations were performed in two different steps, first using the FDM method with a small cluster radius, and later in the multiscattering mode up to larger radius as to include the contribution of the more external shells.

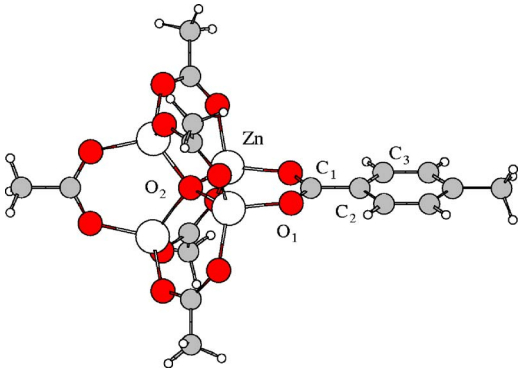


FIG. 4. (Color online) Hydrogenated molecular model system. A close view of a BDC linker connected to a $Zn_4O$ corner. Zn, O, C, and H are shown according to the same color scheme presented in Fig. 1.

All the presented x-ray absorption spectra were calculated self-consistently with a 1*s* core-hole on the absorbing atom and by accounting for by a complete screening. The latter was provided by putting the excited electron on the first empty valence orbital of the absorber. The exchange-correlation term was calculated within the Hedin-Lundqvist approximation, while the Coulomb potential was obtained from the solution of the Poisson's equation. As input data we used the relaxed crystallographic positions and lattice parameters previously described in Sec. III (Table I). Figure 4 shows a fragment of the MOF-5 cluster where all the inequivalent atomic sites are clearly represented.

### A. Oxygen *K*-edge

The oxygen 1*s*-edge (*K*-shell) is obtained when a *s*-core electron is promoted to an excited electronic state, which is coupled with the starting core level through the dipole selection rule ($\Delta\ell = \pm 1$). The oxygen *K*-edge corresponds therefore to the transitions from the *s* core level to the unoccupied *p*-states of the conduction band. The computed XANES spectra of atom type $O_1$ and $O_2$ are shown in Fig. 5. The absorption spectrum of the $O_1$ site is essentially determined by the bonding topology of the Zn-$O_1$-$C_1$ fragment, in which $O_1$ adopts a $sp^2$-planar conformation. In fact, already from the small 3-Å cluster radius calculation performed with the FDM one can see that the absorption edge of $O_1$ consists of two main $\pi^*$ peaks located at the onset energy of the spectrum and a broad $\sigma^*$ signal at higher energy. It is worth noting that when introducing the backscattering contribution of further external shells up to a cluster radius of 10 Å

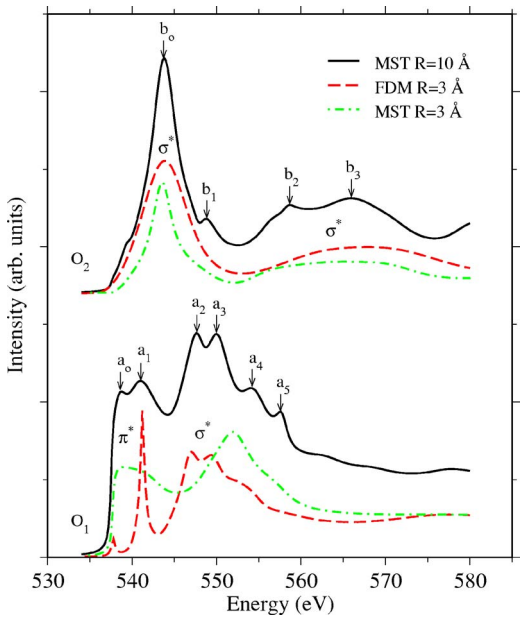


FIG. 5. (Color online) Calculated MST and FDM oxygen *K*-edge spectra. A Lorentzian broadening of 0.2 eV was applied to the computed *K*-edges. A cluster radius ($R$) of 10 Å was found to be large enough for getting well-converged MST XANES spectra, while FDM calculations were performed in a spherical cluster of 3 Å radius. For comparison, a MST spectrum with $R=3$ Å is also shown. A constant energy shift of 7 eV was applied to the Fermi level of both oxygen sites.

(MST), the obtained XANES spectrum changes only slightly. Such a particular effect is ascribed to the cylindrical coordination shell shape of atoms belonging to the BDC linker, for which the influence of a larger spherical atomic cluster is markedly reduced. Hence it is the local geometry imposed by the first coordination shell that determines the primary features of the absorption edge of the $O_1$ site. Our calculated oxygen *K*-edge spectrum can be used as a theoretical spectroscopic reference when trying to discriminate the bonding between the BDC linkers and the $Zn_4O$ corners. The energy positions of the most prominent peaks of this spectrum are listed in Table IV. The computed XAS of $O_2$ is also shown in Fig. 5. The absorption pattern is very much different from that of $O_1$. This can be related to the different composition and geometry of the first coordination shell, which incorporates four Zn ions at a distance of 1.97 Å. Such a chemical coordination reminds one of that of bulk ZnO (Zincite), which has also four Zn ions in its first shell and at the same distance. Because of this, the computed $O_2$ *K*-edge spectrum results are dominated by the same type of $\sigma^*$ states found in pure ZnO crystal.[16] In this case the effect of a larger atomic cluster results clearer than in the case of site $O_1$. A more defined spectrum (see features $b_1-b_3$ of Fig. 5) appears in the larger cluster calculation (MST) because of the characteristic bulklike coordination shells of $O_2$. Note that, when comparing together the spectra of the 3-Å cluster obtained with MST and FDM, one realizes that the latter approach permits one to achieve a more accurate description of the *K*-edge of atom $O_1$, though the $O_2$ spectrum is computed to be very similar in the two calculational schemes. This behavior is attributed to the fact that FDM works better than MST in loosely packed clusters.

TABLE IV. Assignments of peak positions for oxygen and carbon *K*-edges. The energy positions are scaled with respect to the first (low energy) peak of each spectrum. The $\Delta E$ values are given in units of eV.

| $O_1$ | | $O_2$ | | $C_1$ | | $C_2$ | | $C_3$ | |
|---|---|---|---|---|---|---|---|---|---|
| Peak | $\Delta E$ | Peak | $\Delta E$ | Peak | $\Delta E$ | Peak | $\Delta E$ | Peak | $\Delta E$ |
| $a_o$ | 0.0 | $b_o$ | 0.0 | $c_o$ | 0.0 | $d_o$ | 0.0 | $e_o$ | 0.0 |
| $a_1$ | 2.4 | $b_1$ | 5.0 | $c_1$ | 2.4 | $d_1$ | 2.8 | $e_1$ | 3.9 |
| $a_2$ | 9.0 | $b_2$ | 14.8 | $c_2$ | 11.8 | $d_2$ | 5.7 | $e_2$ | 10.5 |
| $a_3$ | 11.3 | $b_3$ | 22.6 | $c_3$ | 15.9 | $d_3$ | 9.9 | $e_3$ | 13.7 |
| $a_4$ | 15.5 | | | $c_4$ | 19.3 | $d_4$ | 15.4 | $e_4$ | 18.0 |
| $a_5$ | 18.9 | | | | | $d_5$ | 19.7 | | |

Despite the evidence that theory provides a clear differentiation between the XAS of $O_1$ and $O_2$, it should be emphasized that the experimental identification of some of the $O_2$ features can be hampered by the relative weight of the atomic sites $O_1$ ($96k$) and $O_2$ ($8c$). The measured oxygen *K*-edge spectrum would likely display a weighted sum of the different oxygen spectra and therefore a predominant contribution from atom $O_1$.

### B. Carbon *K*-edge

In this section we illustrate the calculated carbon *K*-edges of atom types $C_1$, $C_2$, and $C_3$. The obtained XANES are shown in Fig. 6 with the corresponding peak labeling, while their relative energy positions are reported in Table IV. All these spectra are characterized by the presence of the typical $\pi^*$ fingerprints since all the carbon atoms belong to a delocalized system with characteristic double bonds. In particular, atoms $C_2$ and $C_3$ constitute the benzene ring and therefore are directly related to the aromatic circulation, while atom $C_1$ feels both the electronic resonance of the carboxylate group and that of the aromatic ring. As shown in Fig. 4 all these carbon sites belong to the BDC linker, i.e., to the carbon-chain, and therefore they have the same kind of coordination shell packing found for the oxygen $O_1$. As a consequence of this geometry the 3-Å cluster radius calculations (FMD) show a good agreement with the XANES of the 10-Å cluster (MST). The whole *K*-edge pattern reminds one of that of pure graphite where the $\pi^*$ fingerprints dominate the beginning of the carbon edge and the $\sigma^*$ peaks the higher energy region. Identical considerations on the atomic site weights made earlier for the oxygen atoms also apply to these carbon spectra.

## VI. CONCLUSIONS

This paper reports on the *ab initio* investigation of the equilibrium structural parameters, elastic properties, and x-ray absorption near edge spectra of MOF-5 crystal. Good agreement appears to have been reached with experiment

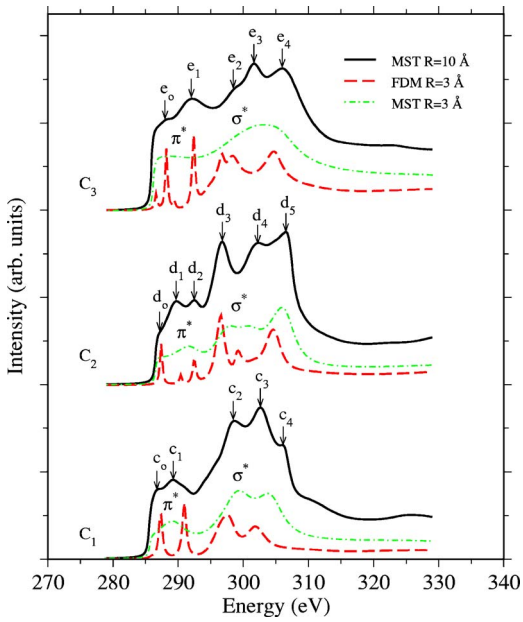


FIG. 6. (Color online) Calculated MST and FDM carbon *K*-edge spectra. The applied Lorentzian broadening is 0.2 eV and the size of the atomic cluster was fixed to a radius of 10 and 3 Å for the MST and to 3 Å for the FDM. A constant energy shift of 5 eV was applied to the Fermi level of all the carbon sites.

regarding the equilibrium geometry and volume. Mechanical properties were described through the computation of the single-crystal elastic constants and by providing important mechanical and technological figures such as Young's modulus, anisotropy factor, Poisson's ratio, sound velocities, and Debye temperature. Contrary to what has been predicted in the very beginning of its discovery, the MOF-5 system is not an *exceptionally rigid structure* but, instead, it behaves as a soft and ductile material.

Lastly, XANES spectra were provided as a spectroscopic reference tool for the characterization and identification of the MOF-5 crystal. Both carbon and oxygen *K*-edges were investigated by means of two different calculational schemes such as the MST and FDM. The calculated oxygen 1*s* shells can be considered as the most important x-ray fingerprints of the MOF-5 material.

## ACKNOWLEDGMENTS

The authors acknowledge the Consejería de Educación de la Comunidad Autónoma de Madrid, the European Social Fund (Contract No. 5813/2002), and the Spanish Ministry of Science (Grant No. BFM 2003-03372) for financial support.

*Present address: Departamento de Física de la Tierra, Astronomía y Astrofísica I, Universidad Complutense de Madrid, E-28040, Spain. Email address: mmattesi@fis.ucm.es

[1] M. Eddaoudi, J. Kim, N. Rosi, D. Vodak, J. Wachter, M. O'Keeffe, and O. M. Yaghi, Science **295**, 469 (2002).
[2] H. Li, M. Eddaoudi, M. O'Keeffe, and O. M. Yaghi, Nature (London) **402**, 276 (1999).
[3] L. Schlapbach and A. Züttel, Nature (London) **414**, 353 (2001).
[4] M. Grätzel, Nature (London) **414**, 338 (2001).
[5] N. L. Rosi, J. Eckert, M. Eddaoudi, D. T. Vodak, J. Kim, M. O'Keeffe, and O. M. Yaghi, Science **300**, 1127 (2003).
[6] O. M. Yaghi, M. O'Keeffe, N. W. Ockwig, H. K. Chae, M. Eddaoudi, and J. Kim, Nature (London) **423**, 705 (2003).
[7] W. Kohn and L. J. Sham, Phys. Rev. **140**, A1133 (1965).
[8] P. Ordejón, E. Artacho, and J. M. Soler, Phys. Rev. B **53**, R10441 (1996).
[9] J. M. Soler, E. Artacho, J. D. Gale, A. Garcia, J. Junquera, P. Ordejón, and D. Sánchez-Portal, J. Phys.: Condens. Matter **14**, 2745 (2002).
[10] J. P. Perdew and A. Zunger, Phys. Rev. B **23**, 5048 (1981).
[11] N. Troullier and J. L. Martins, Phys. Rev. B **43**, 1993 (1991).
[12] L. Kleinman and D. M. Bylander, Phys. Rev. Lett. **48**, 1425 (1982).
[13] O. F. Sankey and D. J. Niklewski, Phys. Rev. B **40**, 3979 (1989).
[14] H. J. Monkhorst and J. D Pack, Phys. Rev. B **13**, 5189 (1976).
[15] J. P. Perdew and M. Levy, Phys. Rev. Lett. **51**, 1884 (1983).
[16] C. L. Dong, C. Persson, L. Vayssieres, A. Augustsson, T. Schmitt, M. Mattesini, R. Ahuja, C. L. Chang, and J.-H. Guo, Phys. Rev. B **70**, 195325 (2004).
[17] W. Y. Ching, M. Z. Huang, Y. N. Xu, W. G. Harter, and F. T. Chan, Phys. Rev. Lett. **67**, 2045 (1991).
[18] J. F. Nye, *Physical Properties of Crystals: Their Representation by Tensors and Matrices* (Oxford University Press, Oxford, 1985).
[19] F. Birch, J. Geophys. Res., [Space Phys.] **83**, 1257 (1978).
[20] M. Mattesini, R. Ahuja, and B. Johansson, Phys. Rev. B **68**, 184108 (2003).
[21] M. Born and K. Huang, *Dynamical Theory of Crystal Lattices* (Clarendon, Oxford, 1956).
[22] W. R. L. Lambrecht, S. Limpijumnong, and B. Segall, MRS Internet J. Nitride Semicond. Res. **4S1**, G6.8 (1999).
[23] J. M. Recio, M. A. Blanco, V. Luaña, R. Pandey, L. Gerward, and J. S. Olsen, Phys. Rev. B **58**, 8949 (1998).
[24] H. J. F. Jansen and A. J. Freeman, Phys. Rev. B **35**, 8207 (1987).
[25] W. Voigt, *Lehrburch der Kristallphysik* (Teubner, Leipzig, 1928).
[26] A. Reuss, Z. Angew. Math. Mech. **9**, 49 (1929).
[27] R. Hill, Proc. Phys. Soc. London **65**, 350 (1952).
[28] S. F. Pugh, Philos. Mag. **45**, 823 (1954).
[29] T. Takasugi and O. Izumi, Acta Metall. **33**, 39 (1985).
[30] T. Takasugi and O. Izumi, Scr. Metall. **19**, 903 (1985).
[31] V. Tvergaard and J. W. Hutchinson, J. Am. Ceram. Soc. **71**, 157 (1988).
[32] B. B. Karki, L. Stixrude, S. J. Clark, M. C. Warren, G. J. Ackland, and J. Crain, Am. Mineral. **82**, 51 (1997).
[33] With the term "isotropic" we intend a material that does not have a preferred orientation.
[34] M. H. Ledbetter, in *Materials at Low Temperatures*, edited R. P. Reed and A. F. Clark (American Society for Metals, Metals

Park, OH, 1983).
[35] V. V. Brazhkin, A. G. Lyapin, and R. J. Hemley, Philos. Mag. Lett. **82**, 231 (1992).
[36] O. L. Anderson, J. Phys. Chem. Solids **24**, 909 (1963).
[37] A. M. Ibrahim, Nucl. Instrum. Methods Phys. Res. B **34**, 135 (1988).
[38] The computer program can be freely downloaded at the address http://www-cristallo.grenoble.cnrs.fr/simulation
[39] Y. Joly, Phys. Rev. B **63**, 125120 (2001).
[40] T. A. Tyson, K. O. Hodgson, C. R. Natoli, and M. Benfatto, Phys. Rev. B **46**, 5997 (1992).
[41] L. Hedin and B. I. Lundqvist, J. Phys. C **4**, 2064 (1971).